JOURNAL OF MATERIALS SCIENCE **35** (2000) 3871–3880

Precipitation in 339 and 2124 aluminum: A caveat for calorimetry

G. W. SMITH, W. J. BAXTER, R. K. MISHRA
General Motors Research and Development Center, Warren, Michigan, USA

The sequence of precipitation in solutionized (SOL) 2124 aluminum and direct-quenched from the die (DQD) 339 aluminum has been identified by a combination of differential scanning calorimetry (DSC) and transmission electron microscopy (TEM). Both alloys form S′ (Al_2CuMg) as the first precipitate after GP zone dissolution. In each alloy a second phase forms at higher temperatures—Si for DQD 339 Al, θ' ($CuAl_2$) for SOL 2124 Al. These results illustrate two difficulties associated with the interpretation of calorimetric observations. 1) The S′ phase precipitates at a much higher temperature in 2124 Al than in 339 Al. Calorimetric determinations of activation energies for GP zone dissolution and S′ precipitation suggest that the former is the rate-determining step for the latter. Since this or similar effects can be expected to control precipitation rates in other alloys, a precipitate is not uniquely identified simply by the DSC peak temperature. Accordingly, the literature must be viewed with caution unless the precipitate assigned to a DSC peak is identified by TEM. 2) As Si forms in DQD 339 aluminum, 40% of the S′ precipitate dissolves. In this circumstance, where two calorimetrically opposed processes occur simultaneously, activation energies determined by differential isothermal calorimetry are erroneous.

1. Introduction

The dominant role of precipitate formation in determining the strength of aluminum alloys is well known. Indeed, this factor has dictated the development of many commercial alloys, encompassing a wide range of alloying elements and hence precipitate compositions. This variety is compounded further by a choice of heat treatments, which for many alloys substantially affects the mechanical properties by virtue of changes in the nature and/or distribution of the precipitates. Thus, an essential key to understanding lies in characterizing precipitate composition, structure, and crystallography. The latter factor defines the precipitate relationship to the host aluminum lattice and hence its effectiveness in strengthening. In essence, the only unequivocal evidence regarding these parameters is provided by transmission electron microscopy (TEM), in combination with associated microanalytic techniques. However, these sophisticated methods are time consuming and not suitable for routine analysis. Furthermore, since the volume of material which can be examined is extremely small, the results may not always be representative of the overall alloy condition.

A simpler and more rapid measure of the precipitation process is provided by differential scanning calorimetry (DSC). This technique uses a larger specimen (∼100 mg) and so provides a more representative macroscopic view. Calorimetry has been applied to investigations of a range of aluminum alloys [1–32]. In a DSC experiment the rate of heat evolution (or absorption) is plotted as a function of temperature, and a precipitation event is manifested as an exothermic peak. For a given heating rate, the peak temperature depends upon the precipitate species and/or the rate-controlling diffusion process. Precipitation kinetics can be determined by various analyses [33–39] which relate the peak temperature to the temperature scan rate. Direct measurements of kinetics can also obtained from differential isothermal calorimetry (DIC) [31, 32].

A major difficulty with DSC is the identification of the precipitate responsible for a specific exothermic peak. In this regard, a survey of the literature indicates that, in general, peaks in the range of 70 to 150 °C are associated with the formation of various GP zones whereas precipitation peaks lie between 200 and 500 °C [2–32]. Nevertheless, there have been disagreements. As Oguocha and Yannacopoulos [28] point out, the literature is not definitive regarding precipitation peak temperatures because of such factors as previous thermal history, material, and DSC heating rate. For example, differences between powder metallurgy and ingot samples have resulted in shifts of peak temperature in alloys 2219 and 6061 [6]. Changing the silicon content in AlMgSi alloys also affects peak temperatures [29]. Sizable differences in various β-phase (Mg_2Si) precipitation peak temperatures in alloy 6061 have been measured by numerous workers [11, 13–15, 19, 20, 24]. Finally, in solutionized alloy 2124 Papazian [6] and Thomas and King [25] detected only a single precipitation peak, which they ascribed to formation of metastable S′ phase (Al_2CuMg), whereas Smith [32] observed a close doublet associated with S′

and θ' ($CuAl_2$). Peak temperature inconsistencies could arise in two ways: (i) if nucleation is not homogeneous but is catalyzed by some extraneous agency, and (ii) if the assignments are not based upon the rigors of TEM correlations. Clearly it is dangerous to assign a given precipitate to a particular DSC peak based solely on a comparison with the literature.

The present paper describes an unambiguous TEM identification of the precipitates responsible for DSC peaks observed in two aluminum alloys: 339 Al direct-quenched from the die (DQD), and 2124 Al which had been solutionized and water-quenched (SOL). In addition, we have applied both DSC and DIC to determine the kinetics parameters (time constants and activation energies) associated with precipitation and dissolution processes in each alloy. These results demonstrate that the interpretation of both DSC and DIC data is not always straightforward.

2. Experimental

2.1. Sample preparation

DQD 339 Al samples were cut from a casting which had been quenched in water after removal from the die and then stored in a freezer at −74 °C prior to sample preparation [40]. The 2124 samples were formed by powder metallurgy (PM) and subsequently solutionized [32]. During fabrication of samples for the DSC experiments, precautions were taken to minimize exposure to ambient temperatures. The DQD 339 samples were removed from the freezer for three brief intervals: (i) initial cutting to rods of square cross section; (ii) machining to cylinders with a diameter of 6 mm; and (ii) slicing discs 2 mm thick. After each step, the samples were returned to the freezer. Preparation of the SOL 2124 samples was simpler because all machining was carried out prior to solution treatment. The samples were solutionized at 495 °C for one hour, quenched in water, then immediately placed in the freezer. Both sets of samples remained in the freezer until one or two minutes before the DSC experiments. The concentrations of the alloying elements, copper, magnesium, and silicon, in each alloy are given in Table I.

2.2. Calorimetry

A Perkin-Elmer DSC7 calorimeter was operated in its temperature-scanned mode to measure the temperature dependence of dQ/dt, the rate of heat absorption or emission by the sample [31, 32]. Such a plot has a baseline proportional to the specific heat of the sample with superimposed endothermic and exothermic peaks due to dissolution and precipitation respectively (e.g., see Fig. 1). The temperature at which a given peak occurs increases with increasing scan rate, from which the activation energy was calculated by the Kissinger method [33, 37]. Identical samples were also measured in the isothermal mode of the calorimeter (e.g., see Fig. 9) to obtain time constants of the exothermic processes. The temperature dependence of these time constants yields a separate measure of the activation energies [31, 32] for comparison with the DSC results. These two methods of analysis are described in more detail below.

TABLE I Concentration of primary alloying elements

	Total concentration (wt %)		
Sample	Cu	Mg	Si
DQD 339 Al	1.04	0.99	∼12
SOL 2124 Al	4.5	1.6	∼0.1

2.3. Transmission electron microscopy

Specimens for TEM were prepared in the calorimeter by heating (at 20 °C/min) to either the first or second precipitation peak, after which they were immediately cooled and stored in the freezer. Four samples prepared in this manner (two each for DQD 339 and SOL 2124) were thinned by mechanical polishing, followed by ion milling. They were then examined in a Philips EM430 scanning transmission electron microscope operating at 300 kV and fitted with a Noran X-ray detector. The precipitates were identified by selected area electron diffraction (SAD), and X-ray microanalysis (XRM) for multiple specimen orientations.

3. Results

3.1. Differential scanning calorimetry

Typical DSC thermal spectra for DQD 339 and SOL 2124 aluminum at a heating rate of 20 °C/min are shown in Fig. 1. In each case several exotherms are visible. As discussed above, we can assign the low temperature exothermic peak to Guinier-Preston (GP) zone formation and the two peaks at higher temperature to precipitation events. The existence of the GP zone peaks indicates that the samples had not been greatly affected by their brief exposure to ambient temperatures during specimen preparation. It is noteworthy that all peaks for the 2124 alloy are much larger than those for 339 Al, reflecting the differences in composition and thermal history. The GP zone formation peaks for both alloys are followed by endotherms which we attribute to dissolution of the GP zones prior to the exothermic precipitation processes. Each alloy exhibits two well

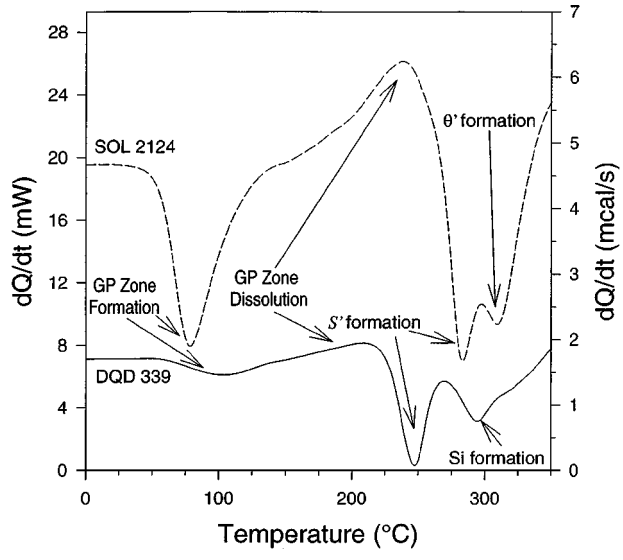

Figure 1 Comparison of DSC scans (at 20 °C/min) for solutionized 2124 Al and direct-quenched from the die 339 aluminum. The temperature of the S′ formation peak for 2124 is about 35 °C higher than that for 339.

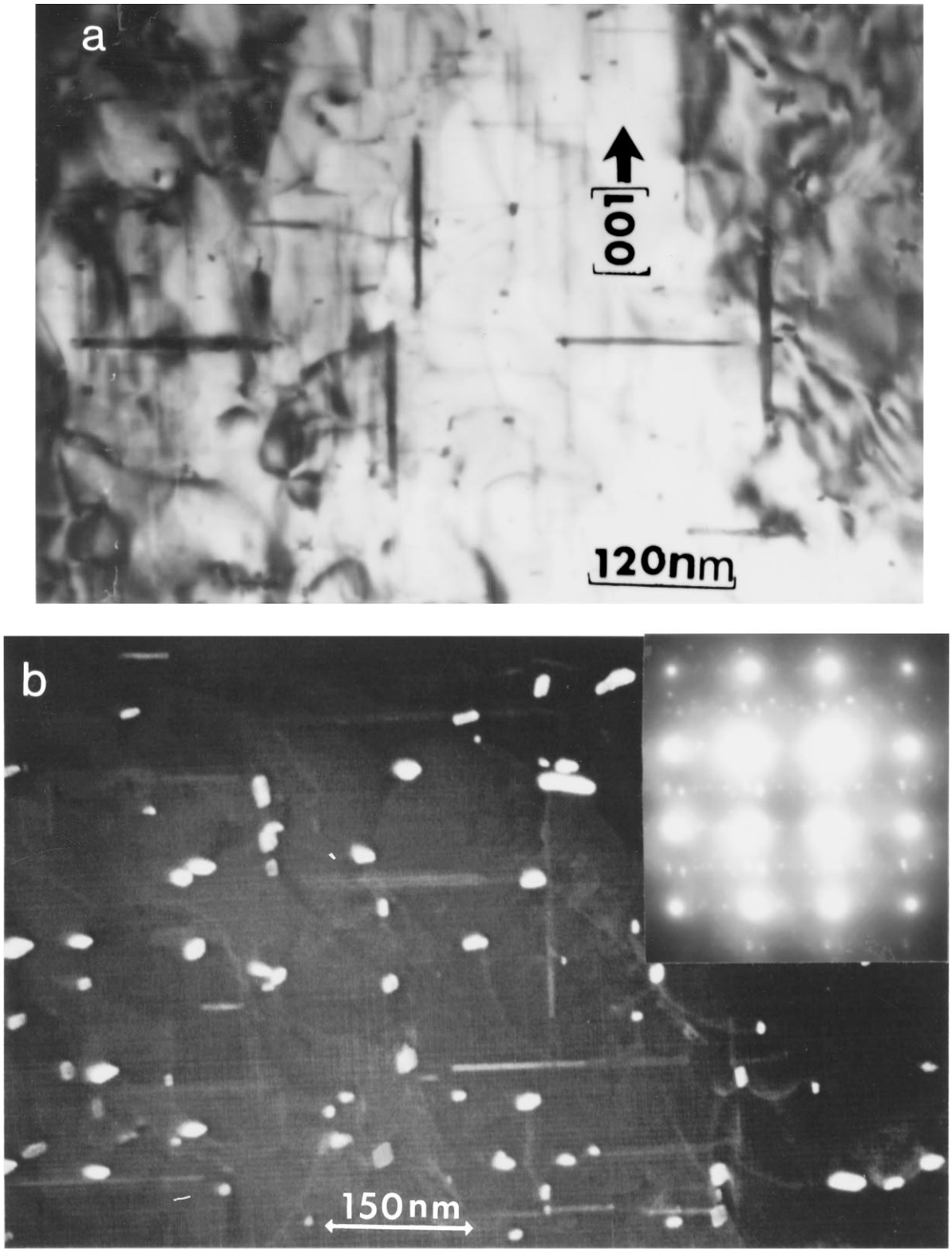

Figure 2 Transmission electron micrographs showing the precipitates in DSC samples of DQD 339 Al: a) after heating to peak at 246 °C and b) after heating to peak at 295 °C.

defined precipitation peaks, but none have a common peak temperature. The precipitates associated with each of these peaks are discussed in the next section.

3.2. Precipitate identification

3.2.1. DQD 339 aluminum

The TEM results for DQD 339 Al have been reported previously [40]. Consequently, we shall briefly summarize those findings.

The sample heated to the first precipitation peak contains primarily thin rod-shaped precipitates about 100 nm long with an aspect ratio larger than 10 (Fig. 2a). The precipitates are coherent with the Al matrix and have a diffraction pattern characteristic of the ternary S′ (Al_2CuMg) phase [41]). No other precipitate phase is present so this peak clearly corresponds to the formation of the S′ phase.

The sample heated to the second DSC peak contains two different phases: (i) rod-shaped S′ phases, and (ii) spherical precipitates of Si [40] as seen in Fig. 2b. Thus the second DSC peak is attributed to formation of the Si phase. But note that the concentration of S′ precipitates

in Fig. 2b is smaller than that in Fig. 2a. In fact, when account is taken of the different thicknesses of these two TEM specimens as determined by convergent beam electron diffraction analysis, the concentration of S′ in the second specimen (Fig. 2b) is about 60% of that in the first specimen (Fig. 2a). Thus the exothermic precipitation of the Si precipitate is accompanied by an endothermic dissolution of some of the S′ precipitates.

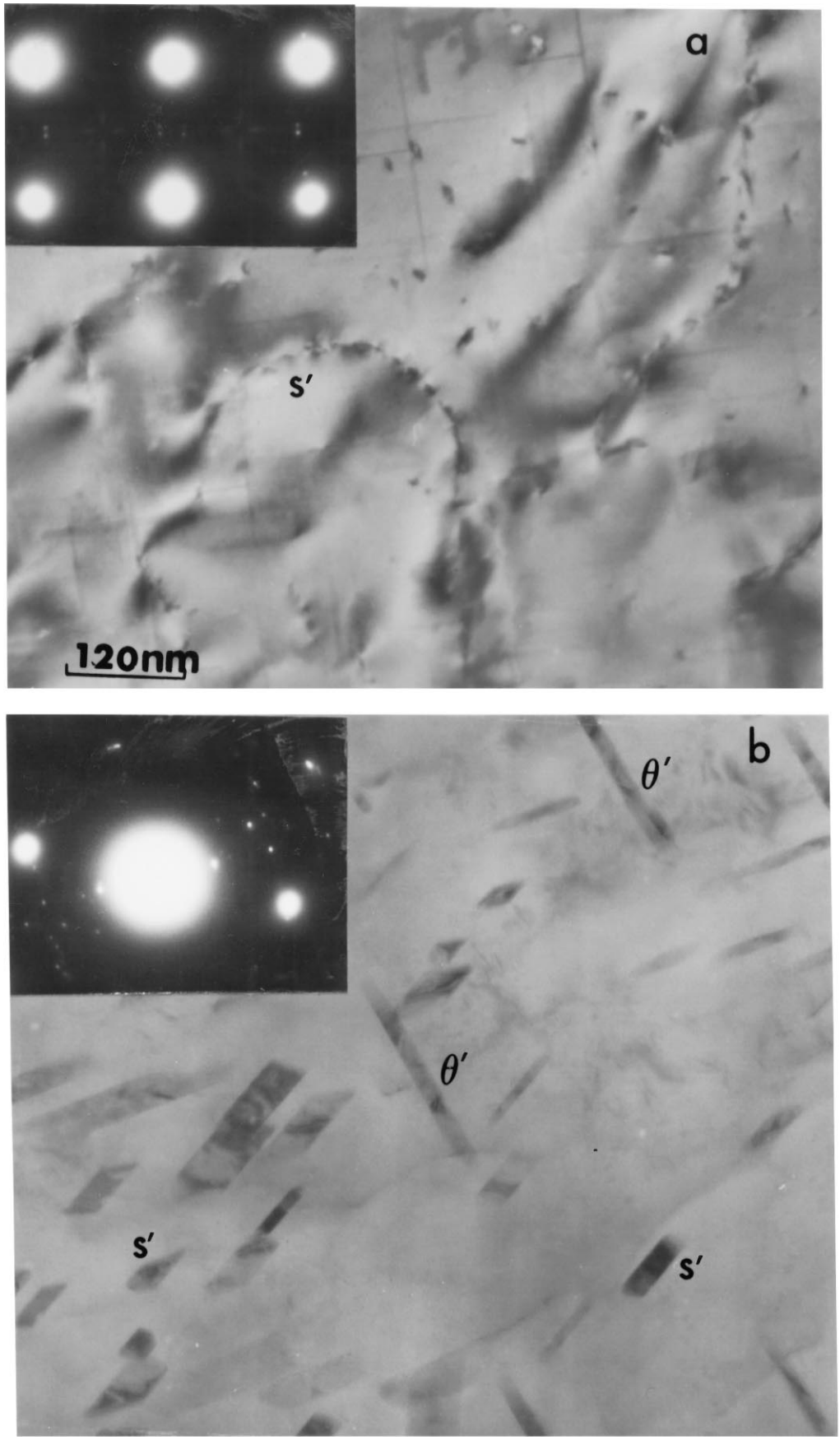

Figure 3 Transmission electron micrographs showing the precipitates in DSC samples of SOL 2124 Al: a) after heating to peak at 284 °C and b) after heating to peak at 309 °C.

3.2.2. SOL 2124 aluminum

Although the precipitates associated with the two peaks have been cited earlier [32], the TEM results on which those assignments are based are reported here for the first time. The identification of precipitates responsible for the first DSC precipitation peak is unambiguous since the sample heated to this peak contained only S′ precipitates, as illustrated by the micrograph in Fig. 3a. The sample heated to the second DSC peak contained not only S′ precipitates, but also the well-known θ' platelets. Note that in this case the concentration of the S′ precipitates is unchanged (cf. Fig. 3a and 3b).

3.3. Precipitation kinetics

3.3.1. Kissinger analyses of DSC spectra

The Kissinger method [33, 37] for deriving activation energies is based on the fact that the temperature, T_p, of a peak increases with increasing scan rate, $S = dT/dt$, as is illustrated in Figs 4 and 5 for DQD 339 Al and SOL 2124 Al. (As is well known, the peak intensity decreases as scan rate is reduced.) The Kissinger equation as modified by Mittemeijer *et al.* [37], is given by:

$$\ln\left(\frac{T_p^2}{S}\right) = \left(\frac{E_{act}}{(RT_p)}\right) + \ln\left(\frac{E_{act}}{Rk_0}\right), \qquad (1)$$

where S is expressed in units of K/s (or °C/s). E_{act} is an effective activation energy, R is the gas constant, and k_0 is the pre-exponential factor in the Arrhenius equation for the rate constant k:

$$k = K_0 \exp\left(\frac{-E_{act}}{RT}\right). \qquad (2)$$

The reciprocal of the rate constant given by Equation 2 is the Kissinger time constant, τ_k [32].

Let us now apply the Kissinger analysis to the various peaks observed for the two alloys in Figs 4 and 5. For each peak we shall plot $\ln(T_p^2/S)$ versus $1/T_p$, the slope of which is proportional to the activation energy (Equation 1). The resulting E_{act} values for the various peaks are summarized in Table II.

3.3.1.1. GP zones. Kissinger plots for the GP zone formation peaks are shown in Fig. 6. Although GP zone formation occurs at lower temperatures in SOL 2124 Al than in DQD 339 Al, the activation energy for the

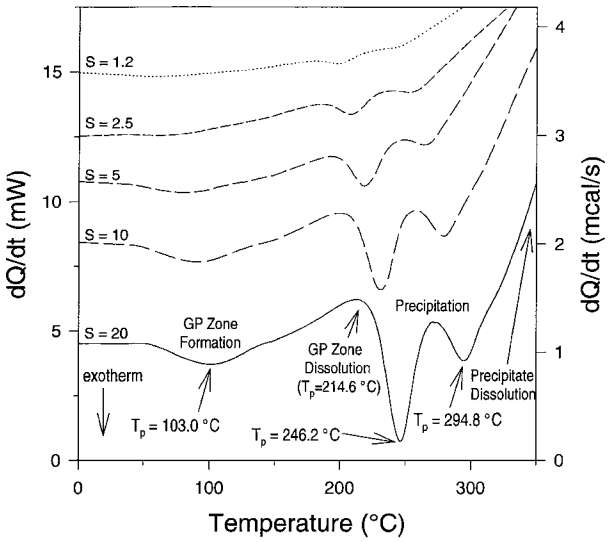

Figure 4 Plots of dQ/dt versus temperature for DQD 339 Al heated at scan rates, S, ranging from 1.2 to 20 °C/min. The curves are shifted vertically to avoid overlap.

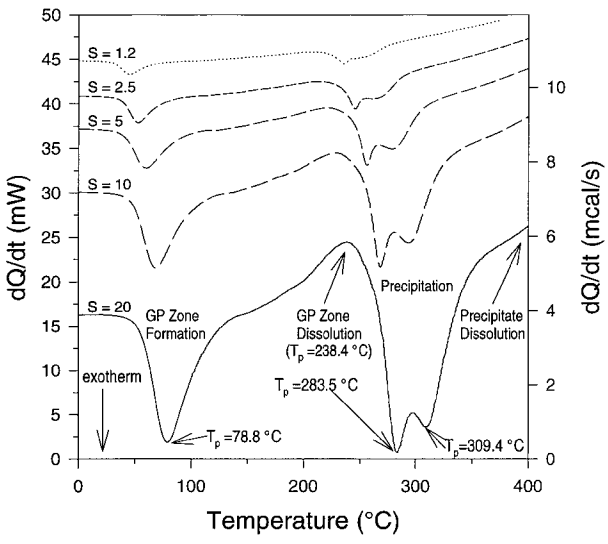

Figure 5 Plots of dQ/dt versus temperature for SOL 2124 Al heated at scan rates, S, ranging from 1.2 to 20 °C/min. The curves are shifted vertically to avoid overlap.

TABLE II Activation energies (kJ/mol)

	SOL 2124 Al		DQD 339 Al	
Process	DSC/ Kissinger	DIC	DSC/ Kissinger	DIC
GP Zone Formation	73 ± 3	76 ± 1	59 ± 1	—
GP Zone Dissolution	150 ± 6	—	123 ± 12	—
S′ Precipitation	131 ± 6	128 ± 15	111 ± 4	91 ± 3
θ' Precipitation	114 ± 5	111 ± 9	—	—
Si Precipitation	—	—	116 ± 5	50 ± 3

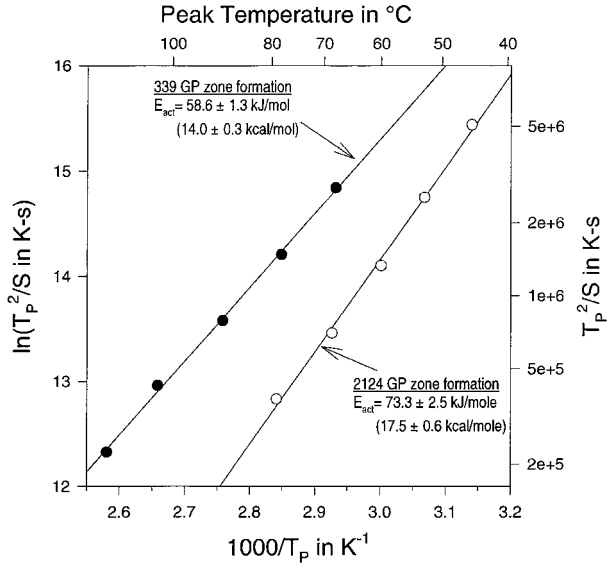

Figure 6 Kissinger plots for the exothermic peak due to GP zone formation in DQD 339 Al and in SOL 2124 Al. The lines are fits of Equation 1.

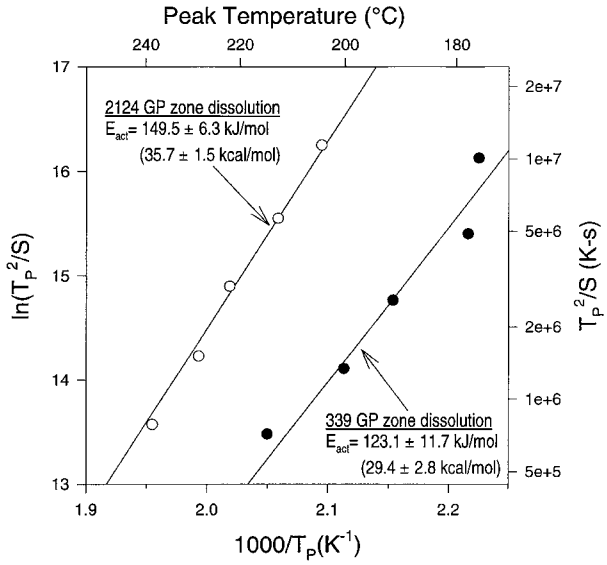

Figure 7 Kissinger plots for the endothermic peak due to GP zone dissolution in DQD 339 Al and in SOL 2124 Al. The lines are fits of Equation 1.

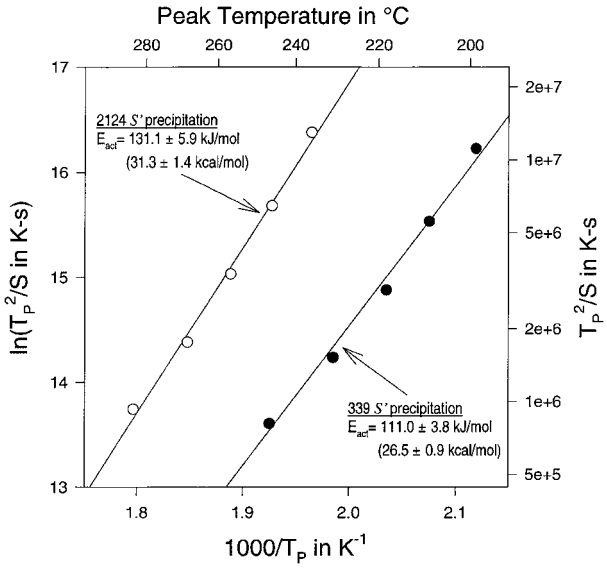

Figure 8 Kissinger plots for the S′ precipitation peak in DQD 339 Al and in SOL 2124 Al. The lines are fits of Equation 1.

former is slightly larger than for the latter. Similar plots for the GP zone dissolution endotherms are shown in Fig. 7. Again we see that E_{act} for 339 Al is lower than the value for 2124 Al and that the dissolution process is faster for 339 Al. These differences in kinetics for both formation and dissolution show that the GP zones in the two alloys are distinctly different.

3.3.1.2. S′ precipitation peaks. The application of the Kissinger analysis requires that X_p, the fraction of species transformed at the peak temperature, should be independent of scan rate [27]. Thus the method must be applied cautiously to doublet peaks, like those of Figs 4 and 5, since this constrain on X_p may be only partially satisfied. However, as indicated in reference 32, the derived values of E_{act} can still be regarded as fairly good approximations. Applying the analysis to the S′ peaks of Figs 4 and 5, we obtain the precipitation time constants shown in Fig. 8 for the two alloys. Clearly the

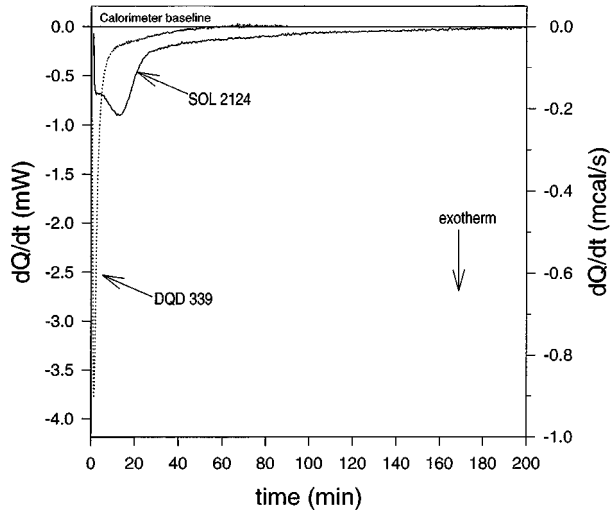

Figure 9 Isothermal calorimetry curves of dQ/dt versus time for precipitation in DQD 339 Al and SOL 2124 Al at 230 °C. As discussed in the text, the decaying portion of each curve is fit well by the sum of two exponentials with time constants τ_1 and τ_2.

activation energy for S′ precipitation in DQD 339 is significantly smaller than in SOL 2124, a somewhat surprising result.

3.3.1.3. Si and θ′ precipitation. For the sake of completeness we include in Table II kinetics results for the high temperature peaks in the two alloys (Si in DQD 339 Al and θ' in SOL 2124). Kissinger plots yield $E_{act} = 116 \pm 5$ kJ/mol for the Si peak in DQD 339 Al, and 113 ± 6 kJ/mol for the θ' peak in SOL 2124 Al.

3.3.2. Analysis of DIC curves

The DIC technique is illustrated in Fig. 9 where dQ/dt, the rate of heat evolution, during precipitation at 230 °C is plotted versus time for both alloys. It is apparent that precipitation occurs in DQD 339 Al much more rapidly than in SOL 2124 Al. Also, two processes are occurring in each case, one fast and one slow, presumably corresponding to the two precipitation events described above. We have applied the 2-exponential analysis technique [31, 32], wherein the decaying portion of the curves are represented by

$$\frac{dQ}{dt} = -\alpha_1 \exp\left(\frac{-t}{\tau_1}\right) - \alpha_2 \exp\left(\frac{-t}{\tau_2}\right). \qquad (3)$$

Arrhenius plots of the time constants τ_1 and τ_2 for precipitation in each alloy are shown in Figs 10 and 11. In each case the fast process (τ_1) is taken to correspond to the low temperature DSC peak, i.e. S′ precipitation, and the activation energies are compared with the Kissinger results in Table II. While the results for SOL 2124 are in good agreement (as previously reported in reference [32], the DIC value for DQD 339 Al is almost 20% lower than that derived from DSC.

In SOL 2124 Al the slower process (τ_2) is taken to correspond to θ' precipitation, and in fact the value of E_{act} from DIC (Fig. 11) is in excellent agreement with that from DSC (Table II). However, in the case of DQD Al 339, the activation energy calculated from τ_2 is only

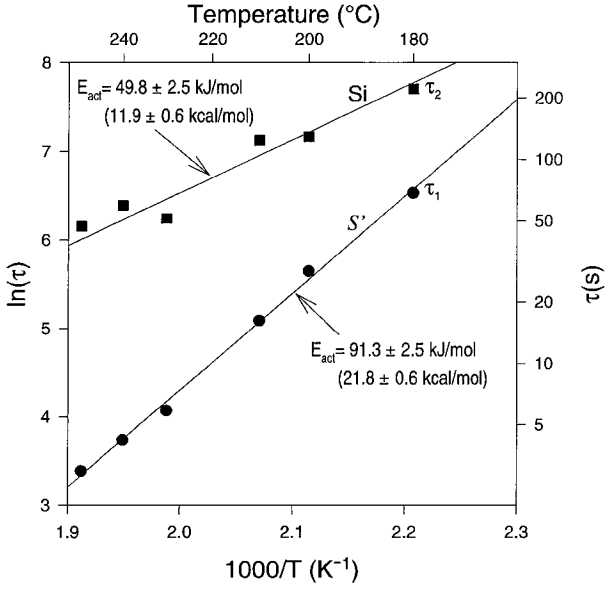

Figure 10 Arrhenius plot of precipitation time constants for DQD Al 339 derived from isothermal curves like that of Fig. 9. The fast precipitation process (τ_1) is associated with the formation of the S′ phase, the slow one (τ_2) with Si precipitation.

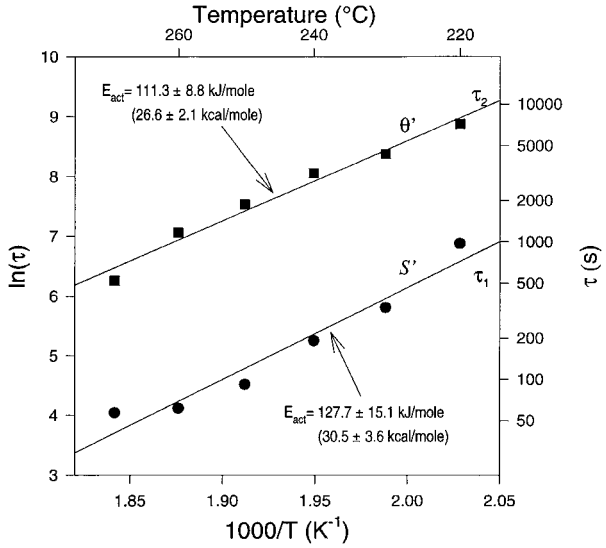

Figure 11 Arrhenius plot of precipitation time constants for SOL Al 2124 derived from isothermal curves like that of Fig. 9. The fast precipitation process (τ_1) is associated with the formation of the S′ phase, the slow one (τ_2) with θ phase formation.

about half that obtained from the Kissinger analysis of the Si precipitation peak.

Finally we include in Table II the DIC result for GP zone formation [32], which is in good agreement with the DSC/Kissinger analysis.

4. Discussion

The combined DSC/TEM studies have clearly shown that the temperature of the S′ peak in SOL 2124 Al is much higher than that in DQD 339 Al. Furthermore, the activation energy, E_{act}, for S′ precipitation in SOL 2124 Al (∼130 kJ/mol) is correspondingly higher than in DQD 339 Al (about 91 to 113 kJ/mol). This disparity indicates that the kinetics are not controlled by an intrinsic process unique to S′ formation, but rather by another process controlling the source of either the copper or magnesium atoms. An obvious candidate is the dissolution of the previously formed GP zones. These not only formed at different temperatures in the two alloys, but more importantly, dissolved at substantially different temperatures as evidenced by the endotherms in Fig. 1. Thus it appears that the formation of the S′ phase awaits GP zone dissolution, and it is the latter process which is the rate-limiting step controlling the kinetics of S′ formation.

Further support for the above conclusion is provided by the activation energies calculated from the Kissinger analysis (Table II). In the case of DQD 339 Al, the activation energy for S′ formation agrees with that for GP zone dissolution. In SOL 2124 Al the activation energy for GP zone dissolution is 14% larger than that for S′ formation. However, it should be noted that in this case the close proximity of the GP zone dissolution endotherm to the S′ precipitation peak may conflict with the constraint on X_p required for the validity of the Kissinger analysis, thus producing a systematic error in the calculated values of E_{act}. Nevertheless, it is evident that the activation energy for S′ precipitation in SOL 2124 Al is ∼16% larger than that in DQD 339 Al, just as the activation energy for GP zone dissolution in SOL 2124 Al is ∼20% larger than in DQD 339 Al.

At this point it is appropriate to compare the values of activation energy derived from the DSC/Kissinger analysis with those calculated from the DIC time constants (Table II). As noted previously [32], in the case of SOL 2124 Al, the values obtained by the two techniques are in excellent agreement for GP zone, S′, and θ' formation. But for DQD 339 Al the DIC values of activation energy are smaller than those obtained from the DSC analysis, particularly for Si precipitation where the DIC activation energy is 60% smaller than the DSC value. We attribute this large discrepancy to the fact that the measured evolution of heat is actually the sum of two simultaneous processes, namely the exothermic precipitation of Si and the endothermic dissolution of S′, as evidenced by the TEM micrographs in Fig. 2. Such a conflict does not occur in SOL 2124 Al where the S′ precipitates remain unchanged during the formation of θ' (Fig. 3), and the activation energies obtained from the DSC and DIC techniques are in excellent agreement.

Thus, for the precipitation of Si in DQD 339 Al the correct value of activation energy is in question. A detailed analysis of the effect of two simultaneous calorimetrically opposed processes on the derived values of E_{act} is obviously beyond the scope of this paper. But we note the following:

i) The DIC value of activation energy is unusually small, whereas the DSC value is comparable to those of all the other processes listed in Table II.

ii) The superposition of an exothermic and an endothermic process will result in a DIC time constant which is some combination of that associated with each process, i.e. the measured time constant and the calculated activation energy will be substantially different from that for Si precipitation.

iii) During a DSC experiment, the major effect of a simultaneous endotherm will be to reduce the observed

magnitude of the precipitation exotherm, with only a minor shift in peak temperature and thereby the calculated activation energy.

For these reasons we believe that for Si precipitation in DQD 339 Al the DSC value of activation energy is reasonably valid, whereas the DIC value is incorrect. On this basis, the precipitation of Si and S′ in DQD 339 Al and θ' in 2124 Al are all controlled by the same activation energy, namely 111 to 116 KJ/mole. This corresponds to the almost identical value of the activation energies for the diffusion of Cu, Si and the self-diffusion of Aluminum [42, 43].

The behavior of the S′ precipitate in these two alloys provides an interesting contrast with important implications for the interpretation of calorimetry in general. In SOL 2124 Al S′ precipitates at a much higher temperature than in DQD 339 Al which we attribute to the different dissolution kinetics of the preceding GP zones. Similarly, the partial dissolution of S′ at 290 °C as Si forms in DQD 339 Al (Fig. 2) contrasts with its total stability at 320 °C as θ' forms in SOL 2124 Al. Interdependencies between various processes of dissolution and precipitation severely complicate the interpretation of calorimetric data. In fact, this study demonstrates that the correct interpretation can only be achieved on the basis of direct observations with TEM.

It is to be expected that similar complications will occur for other precipitate species, depending upon the alloy composition and its thermal history. For example, we have shown [40] that in SOL 339 Al β' (Mg_2Si) precipitates form at ∼240 °C (for $S = 20$ °C/min), i.e., almost the same temperature as the S′ peak in DQD 339 Al (247 °C). But in 6061 Al the β' DSC peak is delayed until ∼300 °C [19, 20]. Again we see the danger of assigning precipitates to DSC peaks solely on the basis of literature comparisons without TEM corroboration. We have reviewed the literature in this regard and summarized our findings in Table III. One obvious discrepancy concerns the DSC peak at ∼290 °C in SOL 339 Al, which was recently attributed to β' by Bar *et al.* [44] on the basis of TEM examination of samples stored at

TABLE III DSC peak temperatures and precipitate assignments for aluminum alloys caveat: For reasons discussed in the text many of the assignments may be incorrect

Precipitate	Alloy	SOL T (°C)	Composition (wt. %) Cu	Mg	Si	Minor Species	Peak T (°C)	Scan Rate (°C/min)	Ppt. Assignment Method	Reference
$CuAl_2$ (θ'', θ')	Al/Cu	520	3.98	0.08	0.07		185, 250	5	TEM	Kim [22]
$CuAl_2$ (θ')	2219 PM	535	(6.3)			(Mn)	300	10	[lit]	Papazian [5]
	2219 ingot	535	(6.3)			(Mn)	279	10	[lit]	Papazian [5]
	2014	490	4.57	0.42	0.66	Fe, Mn, Zn	285	10	TEM	Dutta [23]
	2024	490	4.25	1.3		Fe, Mn	286	20	SEM	Badini [27]
	2124	490	4.5	1.6	0.1		309	20	DSC/TEM	Present work
$CuAl_2$ (θ', θ)	Al/Cu/Mg/Si	495	3.47	0.96	20.2		∼300	10	XRD	Starink [17]
	Al/Cu	520	1.66		0.01		365	20	XRD	Starink [21]
Al_2CuMg (S′)	5182 + Cu	540	1.08	4.36	0.15		∼300	5	TEM	Ratchev [26]
	Al/Cu/Mg	505	1.53	0.79			∼325	10	[lit]	Jena [7]
	2124	505	(4.4)	(1.5)		(Mn)	265	10	[lit]	Thomas [25]
	2124 PM	520	(4.4)	(1.5)		(Mn)	263	10	[lit]	Papazian [5]
	2124 ingot	520	(4.4)	(1.5)		(Mn)	268	10	[lit]	Papazian [5]
	2124	495	4.5	1.6	0.1		284	20	DSC/TEM	Present work
	2024	490	4.25	1.3		Fe, Mn	306	20	SEM	Badini [27]
	2618	500	2.1	1.3	0.03		∼300	20	[lit]	Zahra [12]
	339 DQD	—	1.04	0.99	∼12	Ni, Fe, Mn, Zn	246	20	DSC/TEM	Present work
Mg_2Si (β'')	357	540		0.57	6.97	Sr, Ti	∼250	20	[lit]	Garcia [24]
	6061	540	0.29	1.05	0.62	Fe, Cr, Mn, Ti	264	20	[lit]	Garcia [24]
	6061 PM	530	(.28)	(1)	(0.6)	(Cr)	230	10	[lit] (tentative)	Papazian [5]
	6061 ingot	530	(.28)	(1)	(0.6)	(Cr)	239	10	[lit] (tentative)	Papazian [5]
	6061	540	(.28)	(1)	(0.6)	(Cr)	242	10	DSC/TEM	Dutta [20]
Mg_2Si (β')	Al/Mg/Si	550		0.95	0.85	Zr, Mn	∼255	10	DSC/TEM	Zhen [29]
	357	540		0.57	6.97	Sr, Ti	∼307	20	[lit]	Garcia [24]
	6061	529	0.18	0.84	0.65	Zn	256	20	[lit]	Badini [11, 13–15]
	6061	540	0.29	1.05	0.62	Fe, Cr, Mn, Ti	315	20	[lit]	Garcia [24]
	6061 PM	530	(.28)	(1)	(0.6)	(Cr)	285	10	[lit] (tentative)	Papazian [5]
	6061 ingot	530	(.28)	(1)	(0.6)	(Cr)	289	10	[lit] (tentative)	Papazian [5]
	6061	540	0.24	0.85	0.63	Fe, Cr, Mn	299	10	TEM	Dutta [19]
	6061	540	(.28)	(1)	(0.6)	(Cr)	292	10	DSC/TEM	Dutta [20]
	339	510	1.01	0.78	∼12	Ni, Fe, Mn, Zn	240	20	DSC/TEM	Mishra [40]
	Al/Mg/Cu/Si	480	(1)	(1)	(12)	Ni (∼1%)	290	40	DSC	Bar[44]
Mg_2Si (β)	6061	529	0.18	0.84	0.65	Zn	305	20	[lit]	Badini [11, 13–15]
	6061	540	0.29	1.05	0.62	Fe, Cr, Mn, Ti	∼452	20	[lit]	Garcia [24]
	6061	540	0.24	0.85	0.63	Fe, Cr, Mn	497	10	DSC/TEM	Dutta [19, 20]
	Al/Mg/Si	550		0.95	0.85	Zr, Mn	∼450	10	DSC/TEM	Zhen [29]
$Al_5Cu_2Mg_8Si_6$ (Q)	Al/Cu/Mg/Si	495	3.47	0.96	20.2		238	20	XRD	Starink [17]
Si	339 DQD	—	1.04	0.99	∼12	Ni, Fe, Mn, Zn	295	20	DSC/TEM	Mishra [40]

Notes: Increasing scan rate (e.g. from 10 to 20 °C/min) increases peak temperature by ∼15°C (see, for example, Figs 4 and 5). SOL T: solutionizing temperature. DQD: direct-quenched from the die. PM: powder metallurgy. ( ): nominal compositions. DSC/TEM: DSC scan to peak, followed by TEM analysis; TEM: transmission electron microscopy; SEM: scanning electron microscopy; XRD: X-ray diffraction; [lit]: based on prior literature.

room temperature prior to a DSC experiment. We have shown [40] that this peak is actually due to the precipitation of Si particles. This was unequivocally established by TEM examination of a DSC specimen heated to precisely the peak temperature, a rigorous procedure which we recommend, but which, to our knowledge, has been applied only rarely (Table III). It is also evident from Table III that a majority of the peak assignments rely on comparisons with previous studies. This procedure intrinsically tends to avoid disparities between different alloys, so that consistencies in peak temperatures in Table III may be more apparent than real.

In conclusion, we offer several caveats regarding the interpretation of both DSC and DIC measurements of precipitation, particularly when more than one specie of precipitate can form. In general it appears that more attention should be paid to the endothermic dissolution peaks that precede and can control the kinetics of the exothermic precipitation. (The heat evolved is due to the precipitation event, but the kinetics may be controlled by the preceding dissolution process.) In this case the DSC and DIC data will yield the same activation energy, but it may depend upon the alloy composition. If the endothermic process coincides with exothermic precipitation, DSC and DIC will yield totally different values of activation energy. In this case the DSC value is preferred.

5. Conclusions

Based on the results presented here, the following conclusions may be drawn:

1. The sequence of precipitation in DQD 339 Al and SOL 2124 Al has been identified. The first precipitate to form in both alloys is the S′ (Al_2CuMg) phase, followed at higher temperatures by different precipitates in the two alloys: Si in DQD 339 Al, θ' ($CuAl_2$) in SOL 2124 Al.

2. The precipitation of S′ occurs at a lower temperature in DQD alloy 339 than in SOL alloy 2124. Both DSC Kissinger analysis and DIC determinations show that the apparent activation energy in 339 aluminum is about 15% smaller than in 2124 aluminum.

3. The dissolution of GP zones occurs at a lower temperature in DQD 339 than in SOL 2124, and the activation energy is 18% smaller. It appears that this dissolution process controls the subsequent formation of S′.

4. As Si forms at 290 °C in DQD 339 Al, about 40% of the S′ precipitates dissolve. But as θ' forms at 320 °C in SOL 2124 Al, the S′ precipitates are unaffected.

5. When precipitation coincides with a dissolution process, DIC values of activation energy are invalid.

6. Direct observations by TEM are essential for unequivocal interpretation of DSC precipitation peaks. This is often lacking in the literature, which appears to contain numerous discrepancies.

References

1. K. HIRANO and H. IWASAKI, *Trans. Jap. Inst. Met.* **5** (1964) 162.
2. J. M. PAPAZIAN, *Metall. Trans.* **A12** (1981) 269.
3. M. VAN ROOYAN, J. A. SINTE MAARTENSDIJK and E. J. MITTEMEIJER, *ibid.* **A19** (1988) 2433.
4. C. ANTONIONE, F. MARINO and G. RIONTIONO, *Mater. Chem. Phys.* **20** (1988) 13.
5. S. ABIS and G. DONZELLI, *J. Mater. Sci. Letters* **7** (1988) 51.
6. J. M. PAPAZIAN, *Metall. Trans.* **A19** (1988) 2945.
7. A. K. JENA, A. K. GUPTA and M. C. CHATURVEDI, *Acta. Metall.* **37** (1989) 885.
8. M. C. CHATURVEDI, A. K. GUPTA and A. K. JENA, *Mater. Sci. Eng.* **A110** (1989) 187.
9. M. VAN ROOYAN and E. J. MITTEMEIJER, *Metall. Trans.* **A20** (1989) 1207.
10. I. DUTTA and D. L. BOURELL, *Mater. Sci. Eng.* **A112** (1989) 67.
11. C. BADINI, F. MARINO and A. TOMASI, *Mater. Chem. Phys.* **25** (1990) 57.
12. A.-M. ZAHRA and C. Y. ZAHRA, *J. Thermal Anal.* **36** (1990) 1465.
13. C. BADINI, F. MARINO and A. TOMASI, *Mater. Sci. Eng.* **A136** (1991) 99.
14. *Idem., J. Mater. Sci.* **26** (1991) 6279.
15. P. APPENDINO, C. BADINI, F. MARINO and A. TOMASI, *Mater. Sci. Eng.* **A135** (1991) 275.
16. M. J. STARINK and P. VAN MOURINK, *Metall. Trans* **A20** (1991) 665.
17. M. J. STARINK, V. JOORIS and P. VAN MOURINK, in "Metal Matrix Composites—Processing, Microstructure and Properties," edited by N. Hansen, D. Juul Jensen, T. Leffers, H. Lilholt, T. Lorentzen, A. Schrøder Pedersen, O. B. Pedersen and B. Ralph, (Risø National Lab, Roskilde, Denmark, 1991), p. 675.
18. H.-L. LEE, W.-H. LU, S. L.-I. CHAN, *Scripta Metall. Mater.* **25** (1991) 2165.
19. I. DUTTA, S. M. ALLEN and J. L. HAFLEY, *Metall. Trans.* **A22** (1991) 2553.
20. I. DUTTA and S. M. ALLEN, *J. Mater. Sci. Letters* **10** (1991) 323.
21. M. J. STARINK and P. VAN MOURINK, *Mater. Sci. Eng.* **A156** (1992) 183.
22. T. S. KIM, T. H. KIM, K. H. OH and H. I. LEE, *J. Mater. Sci.* **27** (1992) 2599.
23. I. DUTTA, C. P. HARPER and G. DUTTA, *Metall. Mater. Trans.* **A25** (1994) 1591.
24. C. GARCIA-CORDOVILLA, E. LOUIS, J. NARCISO and A. PAMIES, *Mater. Sci. Eng.* **A189** (1994) 219.
25. M. P. THOMAS and J. E. KING, *J. Mater. Sci.* **29** (1994) 5272.
26. P. RATCHEV, B. VERLINDEN and P. VANHOUTE, *Scripta Metall. Mater.* **30** (1994) 599.
27. C. BADINI, F. MARINO and E. VERNE, *Mater. Sci. Eng.* **A191** (1995) 185.
28. I. N. A. OGUOCHA and S. YANNACOPOULOS, *ibid.* **A231** (1997) 25.
29. L. ZHEN, W. D. FEI, S. B. KANG and H. W. KIM, *J. Mater. Sci.* **32** (1997) 1895.
30. M. J. STARINK and A.-M. ZAHRA, *Phil. Mag.* **76** (1997) 701.
31. G. W. SMITH, *Thermochimica Acta* **313** (1998) 27.
32. *Idem., ibid.* **317** (1998) 7.
33. H. E. KISSINGER, *Anal. Chem.* **29** (1957) 1702.
34. T. OZAWA, *J. Thermal Anal.* **2** (1970) 301; **3** (1973) 501; **7** (1975) 601; *Bull. Chem. Soc. Japan* **57** (1984) 639.
35. R. L. THAKUR, in "Advances in Nucleation and Crystallization of Glasses," edited by L. L. Hench and S. W. Freiman (Amer. Ceram. Soc., Columbus, OH, 1972), p. 166 (cited in reference [36]).
36. J. A. AUGIS and J. E. BENNETT, *J. Therm. Anal.* **13** (1978) 283.
37. E. J. MITTEMEIJER, L. CHENG, P. J. VAN DER SCHAAF, C. M. BRAKMAN and B. M. KOREVAAR, *Metall. Trans.* **A19** (1988) 925.
38. H. YINNON and D. R. UHLMANN, *J. Non-Crystalline Solids* **54** (1983) 253.
39. J. SESTAK, in "Comprehensive Analytical Chemistry, Vol. XII, Part D," edited by G. Svehla (Elsevier, Amsterdam, 1984) Ch. 9, p. 212.

40. R. K. MISHRA, G. W. SMITH, W. J. BAXTER, A. K. SACHDEV and V. FRANETOVIC, submitted for publication.
41. A. K. GUPTA, P. GAUNT and M. C. CHATURVEDI, *Phil. Mag.* **55** (1987) 375.
42. T. S. LUNDY and J. F. MURDOCK, *J. Appl. Phys.* **33** (1962) 1671.
43. P. M. BEYELER and Y. ADDA, *Le Journal de Physique* **29** (1968) 345.
44. J. BAR, H.-J. GUDLADT, J. ILLY and J. LENDVAI, *Mat. Sci. Eng.* **A248** (1998) 181.

Received 28 May 1999
and accepted 19 January 2000